Symmetry properties of fluctuations in an actively driven rotor

Symmetry properties of fluctuations in an actively driven rotor*

He Li(李赫),[1,†] Xiang Yang(杨翔),[1] and H. P. Zhang(张何朋)[1,2,†]

[1] *School of Physics and Astronomy and Institute of Natural Sciences, Shanghai Jiao Tong University, Shanghai 200240, China*

[2] *Collaborative Innovation Center of Advanced Microstructures, Nanjing, China*

We investigate rotational dynamics of an actively driven rotor through experiments and numerical simulations. While probability density distributions of rotor angular velocity are strongly non-Gaussian, relative probabilities of observing rotation in opposite directions are shown to be linearly related to angular velocity magnitude. We construct a stochastic model to describe transitions between different states from rotor angular velocity data and use the stochastic model to show that symmetry properties in probability density distributions are related to detailed Fluctuation Relation (FR) of entropy productions.

Keywords: Brownian motor, active bath, fluctuation relation, active matter

PACS: 05.40.-a, 05.60.-k, 05.70.Ln

I. INTRODUCTION

When a particle is dragged through a heat bath by an external force, it occasionally moves in the opposite direction to the external force. Such entropy consuming events have been shown to obey the fluctuation relation [1, 2]. Fluctuation relations, which go beyond the traditional second law of thermodynamics, express the relative possibility to find entropy production and entropy consuming events in small-scale non-equilibrium systems. Its validity has been proved in a surprising range of experiments [3–6], even extended to several non-thermal systems nominally outside their realm of applicability [7–14].

Active matter systems consist of individual particles which can move by consuming energy and converting it into self-propulsion force [15–20]. Such a self-propulsion mechanism drives system out of equilibrium, and is typically noisy in itself [21]. Random motions of active particles often work as "active bath" [22, 23], and provide athermal fluctuations for passive particle immersed in the system. It is a intrigue question to ask whether microscopic thermodynamic laws such as fluctuation relations hold in active bath [24–26].

In this paper, we present a statistical analysis of angular velocity fluctuations of an asymmetric rotor driven by self-propelled robots. Our main results are as follows: (1) rotor angular velocities, from both experiments and numerical simulations, have strongly non-Gaussian distributions; (2) relative probability for the rotor to rotate in positive and opposite directions is related to the averaged angular velocity magnitude in a period of time; (3) symmetry properties in probability density distributions are related to detailed Fluctuation Relation (FR) of entropy productions at the trajectory level.

II. EXPERIMENT

Our experimental setup is shown in Fig. 1(A), consisting of an asymmetric rotor and self-propelled robots. The rotor is cut from 2-cm-thick styrofoam sheet by a CNC foam cutter. Outer radius of the rotor is 11.5 cm, and the radius of 8 inner corners of the rotor is 8.5 cm. Part of the interior material is removed to reduce the rotor mass and finally each rotor weights around 8 g. The rotor is connected to an axis fixed to the bottom styrofoam board by two low-friction ceramic ball bearings.

Robots, serving as heat bath in our experiments, are commercially available toys, Hexbug, whose body is 4.3 cm long and 1.2 cm wide. Each robot is driven by a vibration motor. Robot moves with intrinsic rotation and translation noise, which are approximately Gaussian [27]. As shown in Fig. 1(A), robots are placed in an circular experiment cell, with flower-shaped acrylic boundary. Moving robots interact with the rotor through inelastic collision. Upon collision, robots lose their velocity components normal to the rotor boundary and begin to slide along the surface. Such inelastic collisions drive asymmetric rotor into unidirectional motion (CCW) with apparent fluctuations, see Fig. 1(B).

Motion of the rotor and robots is recorded by a high-speed camera placed vertically above the experiment arena, with a resolution of 900×900 pixel^2 over a field of view of 50×50 cm^2. The frame rate used is 20 fps and each video is 1000s long. Reflective sheets are attached to both rotor's edge and robots to increase the contrast. We use a standard particle tracking algorithm to locate and track the reflective markers. Velocity of each marker is computed as the difference of location between two successive images. And rotor's angular velocity in each step, Ω, is obtained by averaging the angular velocities, relative to center axis, of the 8 markers on the rotor. We cut the raw angular velocity time series into segments

* Project supported by the National Natural Science Foundation of China (No. 11422427, 11402069), the Program for Professor of Special Appointment at Shanghai Institutions of Higher Learning (No. GZ2016004).

† Corresponding author. E-mail:hepeng_zhang@sjtu.edu.cn, liheg36ke@gmail.com

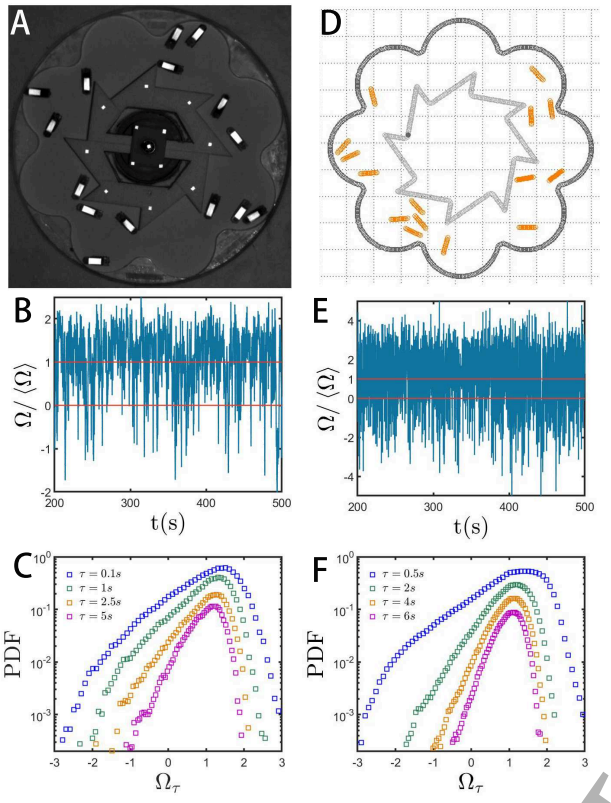

FIG. 1. Setup (A, D), temporal record of rotor velocity (B, E) and probability distribution of averaged rotor velocity (C, F) from experiments (left column, (A-C)) and numerical simulations (right column, (D-F)). (A, D) System composed of an asymmetric rotor and self-propelled robots. Flower-shape acrylic boards are used to prevent robots from sticking on the outside boundary. (B, E) Temporal fluctuations around averaged rotation velocity of the rotor. (C, F) Probability distribution functions of averaged angular velocity Ω_τ.

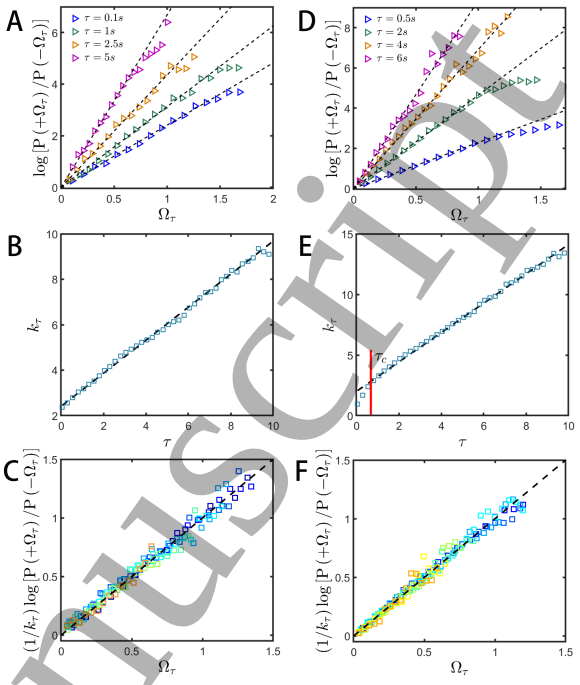

FIG. 2. Symmetry function $\log\left[\mathrm{P}\left(+\Omega_\tau\right)/\mathrm{P}\left(-\Omega_\tau\right)\right]$ (A, D), slope of symmetry function (B, E), and rescaled symmetry function (C, F) from experiments (left column, A-C) and simulations (right column, D-F).

of 200s long. Mean value of angular velocity and corresponding distribution in each time interval are stable after the beginning 200s. We then exclude the first 200s interval, and use remaining data for statistical analysis.

We define a time averaged angular velocity over a time interval τ, $\Omega_\tau(t) = (1/\tau)\int_t^{t+\tau}\left[\Omega(t')/\langle\Omega\rangle\right]\mathrm{d}t'$, where $\langle\cdot\rangle$ denotes an average over the entire time series, and $\mathrm{P}(\Omega_\tau)$ denotes its probability distribution function (PDF).

A typical time series and PDF of angular velocity for a rotor driven by 15 robots are shown in Fig. 1(B) and (C). Both positive and negative fluctuations around mean value are observed. In order to calculate time series of Ω_τ, we divide the $\Omega/\langle\Omega\rangle$ series into bins of length τ, and average over overlapping bins where the center of each bin is shift from the previous one by a time difference 0.05s, to improve statistics. Probability distribution functions of coarse-grained angular velocity for different integration time $\tau = 0.1s, 1s, 2.5s, 5s$ are presented in Fig. 1(C). One could see that these PDFs are non-Gaussian even after long time integration. Motivated by findings in [12, 14], we then examine the relative probabilities of positive and negative coarse-grained angular velocity Ω_τ. We are surprised to find the symmetry functions $F(\Omega_\tau) = \log\left[\mathrm{P}\left(+\Omega_\tau\right)/\mathrm{P}\left(-\Omega_\tau\right)\right]$ are almost linearly related to Ω_τ for $\tau = 0.1s, 1s, 2.5s$ and $5s$, with a slope k_τ increasing almost linearly with τ as shown in Fig. 2, consistent with results in [4, 5, 7, 29, 30]. Symmetry functions deviate from linear relation at large angular velocity values, where the amount of data is often insufficient.

III. NUMERICAL SIMULATION

To investigate the necessary factors that lead to the non-Gaussian fluctuations and unusual symmetry properties, and to explore their existence in a wider parameter space, we create a simulation model composed of self-propelled rods and a rotary rotor, see Fig. 1(D). Rods are constructed by 5 overlapping spheres joined along a straight line and their sizes are chosen according to width of Hexbug robots used in experiments. All spheres from different rods interact with each other via a Yukawa potential. Flower-shaped boundary and the rotor are constructed from a string of the same kind of spheres.

In simulations, center-of-mass $\mathbf{r}(t)$ and orientation angle $\theta(t)$ of a rod are controlled by second order Langevin

Table I. Parameters in numerical simulations.

$I\left(g\cdot cm^2\right)$	1500
$\alpha_I\left(N\cdot cm\cdot s\right)$	0.015
$m_0\left(g\right)$	7
$f_{sp}\left(N\right)$	0.2
$\alpha_0\left(N\cdot cm^{-1}\cdot s\right)$	0.01
$D_0\left(N^2\right)$	0.00002
$I_0\left(g\cdot cm^2\right)$	10
$\alpha_{I0}\left(N\cdot cm\cdot s\right)$	0.001
$D_{I0}\left(N^2\cdot cm^2\right)$	0.00001

equations:

$$m_0\frac{\mathrm{d}^2\mathbf{r}}{\mathrm{d}t^2}=\mathbf{f}_{ex}+\mathbf{f}_{sp}-\alpha_0\frac{\mathrm{d}\mathbf{r}}{\mathrm{d}t}+\sqrt{2D_0}\xi_r\left(t\right) \tag{1}$$

$$I_0\frac{\mathrm{d}^2\theta}{\mathrm{d}t^2}=\tau_{ex}-\alpha_{I0}\frac{\mathrm{d}\theta}{\mathrm{d}t}+\sqrt{2D_{I0}}\xi_\theta\left(t\right), \tag{2}$$

where m_0 and I_0 are mass and moment of inertia of each rod, and translational and rotational noise term are included to capture the naturally existing fluctuation in robots' velocity and moving directions [27]. ξ_r and ξ_θ are standard Gaussian noise. Translational and rotational noise are not fundamentally coupling for dry active particles [28], and their magnitudes are controlled by diffusion coefficient D_0 and D_{I0}, which are separately determined by experiment measurements. $\mathbf{f}_{ex}$ and τ_{ex} denote external force and torque from other rods and boundary, α_0 and α_{I0} are friction coefficients. Energy is injected into the system through self-propelled force $\mathbf{f}_{sp}$ acting on the last particle of each rod and parallel to rod body, which ensures the rod easily slides along rotor boundary after collision. This detail is important to repeat apparent uni-directional rotation observed in experiment. Change of rotor angle Θ is described by the following equation:

$$I\frac{\mathrm{d}^2\Theta}{\mathrm{d}t^2}=T_{ex}-\alpha_I\frac{\mathrm{d}\Theta}{\mathrm{d}t}, \tag{3}$$

where I is moment of inertia of the rotor, and friction coefficient α_I is set to a very low value to simulate the low-friction ball bearing in experiment. Rotational noise term is excluded in Eq. 3 because the gear is a macroscopic object and doesn' t show any spontaneous fluctuations. T_{ex} is the total torque due to collisions with self-propelled rods. Parameters values used in simulation are listed in Table 1. With these parameters, our numerical model can reproduce experimental results in angular velocity statistics (right column of Fig. 1) and symmetry functions (right column of Fig. 2). We explored the effect of the shape of the central gear, and magnitude of self-propelling force $\mathbf{f}_{sp}$, and found the non-Gaussian

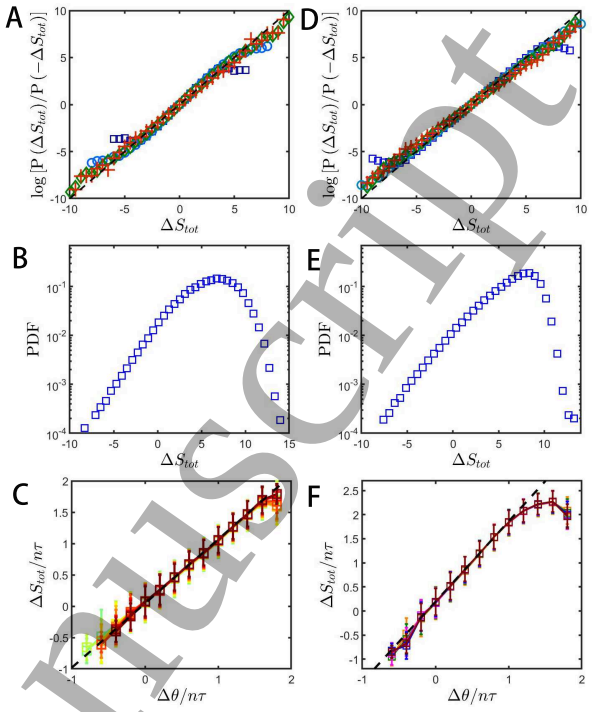

FIG. 3. (A) Detailed fluctuation relation of total entropy production ΔS_{tot} for different trajectory length $n\tau$. Colors and markers shapes present time length of trajectories. dark blue squares: $n\tau=2s$, light blue circles: $n\tau=4s$, green diamonds: $n\tau=6s$, red daggers: $n\tau=8s$. (B) Probability distribution functions of total entropy production ΔS_{tot} ($n\tau=6s$). (C) Total entropy production ΔS_{tot} versus angular displacement $\Delta\theta$. Data are divided by $n\tau$ for the convenience of comparison. Corresponding simulation results are presented in (D-F).

shape and symmetry properties of rotor angular velocity distributions are qualitatively maintained. Fig. 2(E) shows that linear dependence of slope k_τ vs τ is valid in simulation when $\tau\geq 0.5s$ (Fig. 2(E)). Characteristic time scale of one self-propelling rod colliding and pushing the rotor is approximately 0.3-0.5s, which is comparable to this critical time scale τ_c. It requires further investigations in the future to determine whether these two timescales are fundamentally related.

IV. ENTROPY PRODUCTION

We use the idea of entropy production [2, 31] to further our understanding of symmetry functions in Figs. 1 and 2. To compute entropy production along a trajectory, we need to know the transition probability between states. To that end, a discrete time Markovian model for angular velocity time series Ω_τ is constructed for coarse-grain time larger than typical rotor-robot collision time ($0.5s$). For example, we can coarse-grain typical data set (c.f. Fig. 1(B)) with an average time $\tau=0.5$ s, then calculate difference in two successive steps $d\Omega_{\tau n}=\Omega_{\tau(n+1)}-\Omega_{\tau n}$

as the acceleration at time step n. After binning angular velocity time series Ω_τ to 26 discretized states Ω_i, we then can easily calculate PDF of acceleration for each specific state $\mathrm{P}_a\left(\mathrm{d}\Omega_\tau|\Omega_i\right)$. In the end $\mathrm{P}_a\left(\mathrm{d}\Omega_\tau|\Omega_i\right)$ severs as a discrete time, discrete state stochastic model for rotor's angular velocity.

Based on this stochastic description of angular velocity evolution, we can calculate trajectory-dependent total entropy production, ΔS_{tot}, as defined in [2, 31], for any trajectory of time length $n\tau$. Here we directly follow the method in [32, 33] since angular velocity is of odd-parity under time reversal operation. Let $x\left(n\tau\right)$ denotes a trajectory of length $n\tau$, $\left(\Theta_0,\Omega_{\tau 0}\right),\left(\Theta_1,\Omega_{\tau 1}\right)\cdots,\left(\Theta_n,\Omega_{\tau n}\right)$, and $x^\dagger\left(n\tau\right)$ presents its time reversal process, $\left(\Theta_n,-\Omega_{\tau n}\right),\left(\Theta_{n-1},-\Omega_{\tau n-1}\right)\cdots,\left(\Theta_0,-\Omega_{\tau 0}\right)$. $\Omega_{\tau i}$ denotes the coarse-grained angular velocity at time $t=i\tau$,(n and i are integers). Probability of observing trajectory $x\left(n\tau\right)$ is given by $\mathrm{P}\left[x\left(n\tau\right)\right]=\mathrm{p}_0\left(\Theta_0,\Omega_{\tau 0}\right)\mathrm{p}\left(\Theta_1,\Omega_{\tau 1}|\Theta_0,\Omega_{\tau 0}\right)\cdots\mathrm{p}\left(\Theta_n,\Omega_{\tau n}|\Theta_{n-1},\Omega_{\tau n-1}\right)$. p_0 denotes the initial distribution, and $\mathrm{p}\left(\Theta_i,\Omega_i|\Theta_j,\Omega_j\right)$ is a transition probability between two states, which equals to $\mathrm{P}_a\left(\Omega_i-\Omega_j|\Omega_j\right)$ given by our stochastic model. Since our system has rotationary symmetry, position Θ_0 dependence can be neglected and the above expression could be easily written in the following shorter form

$$\mathrm{P}\left[x\left(n\tau\right)\right]=\mathrm{p}_0\left(\Omega_{\tau 0}\right)\mathrm{p}\left(\Omega_{\tau 1}|\Omega_{\tau 0}\right)\cdots\mathrm{p}\left(\Omega_{\tau n}|\Omega_{\tau n-1}\right). \tag{4}$$

And its reverse path $x^\dagger\left(n\tau\right)$ is constructed by initiating at the end of the forward process, reversing the sign of angular momentum, and evolving backward in time. We have

$$\begin{aligned}\mathrm{P}\left[x^\dagger\left(n\tau\right)\right]=&\,\mathrm{p}_0^\dagger\left(-\Omega_{\tau n}\right)\mathrm{p}\left(-\Omega_{\tau n-1}|-\Omega_{\tau n}\right)\\&\cdots\mathrm{p}\left(-\Omega_{\tau 0}|-\Omega_{\tau 1}\right).\end{aligned} \tag{5}$$

The total entropy production is defined as the logarithm of the ratio between the probabilities of the trajectory and its time-reversed counterpart $\Delta S_{tot}=\log\left(\frac{\mathrm{P}[x(n\tau)]}{\mathrm{P}[x^\dagger(n\tau)]}\right)$. Entropy production characterizes the irreversibility of the forward path. According to how the reverse trajectory is defined, we choose initial probability of reverse path $\mathrm{p}_0^\dagger\left(-\Omega_{\tau n}\right)$ as the final probability of the forward process $\mathrm{p}_n\left(\Omega_{\tau n}\right)$, as mentioned in [33]. Changes in trajectory entropy $\log\left(\frac{\mathrm{p}_0(\Omega_{\tau 0})}{\mathrm{p}_n(\Omega_{\tau n})}\right)$, which equals to $\log\left(\frac{\mathrm{p}_0(\Omega_{\tau 0})}{\mathrm{p}_0^\dagger(-\Omega_{\tau n})}\right)$, is naturally included in the definition. Since rotor rotation reaches a steady state in our case, we set both initial and final distributions of Ω_τ as the steady state distribution $\mathrm{p}_0\left(\Omega_\tau\right)=\mathrm{p}_n\left(\Omega_\tau\right)=\mathrm{P}\left(\Omega_\tau\right)$, which has been provided in Fig. 1(C)(F).

Given a trajectory consisting of a series of n $\Omega_{\tau i}$, we first allocate each value into corresponding discrete state, and calculate the probability of forward and backward process using Eq. 4 and Eq. 5. We can then calculate entropy production for each trajectory. The linear fluctuation relation $\log\frac{\mathrm{P}(\Delta S_{tot})}{\mathrm{P}(-\Delta S_{tot})}=\Delta S_{tot}$ is found to be satisfied for any trajectory time length (Fig. 3(A)). This result in turn proves validity of the model we use to describe the rotor's motion. PDF of ΔS_{tot} is non-Gaussian, similar to distribution of angular velocity (Fig. 3(B)). The same technique can be applied to simulation data. Linear relation with slope 1 and non-Guassian PDF for ΔS_{tot} are also observed in numerical result (Fig. 3(D)(E)).

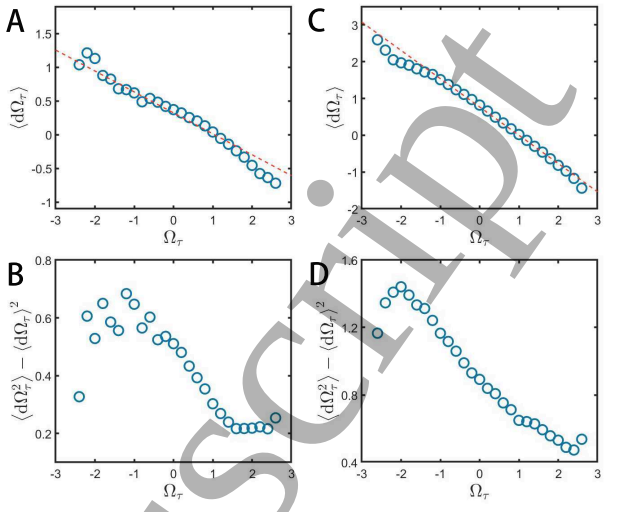

FIG. 4. Mean (A, C) and variance (B, D) of rotor acceleration $\mathrm{d}\Omega_\tau$ depends on rotor velocity. As in previous figures, experimental and numerical results are plotted in left and right column, respectively.

V. PHYSICAL SIGNIFICANCE OF STOCHASTIC ENTROPY PRODUCTION

To illustrate the significance of computed entropy production, we now turn to the connection between ΔS_{tot} and angular displacement $\Delta\theta$ for a specific trajectory. For a given trajectory length $n\tau$, we calculate average value and standard deviation of ΔS_{tot} for all trajectories with a specific angular displacement $\Delta\theta$. We plot $\Delta S_{tot}/n\tau$ against $\Delta\theta/n\tau$ in Fig. 3(C). Here we divide both of quantities by $n\tau$ to put data from different trajectory length on the same plot. Note that $\Delta\theta/n\tau$ is exactly the average angular velocity $\Omega_{n\tau}$. We find that data collapse for long trajectories ($n\tau\geqslant 6s$) and an almost linear relation between $\Delta S_{tot}/n\tau$ and $\Delta\theta/n\tau$ (i.e. $\Omega_{n\tau}$) appears, with a slope factor not equal to 1. This fact shows that, in our system, the average angular velocity during a period of time, can server as a direct indication of irreversibility. It also explains the FR-like linear dependency shown in Fig. 2.

Statistics of angular acceleration contains important information. As shown in Fig. 4(A)(C), average value of $\mathrm{d}\Omega_\tau$ decreases almost linearly with rotation velocity Ω_τ , suggesting a linear drag term in the governing equation. The variance of $\mathrm{d}\Omega_\tau$, $\left\langle {d\Omega_\tau}^2\right\rangle$-$\left\langle d\Omega_\tau\right\rangle^2$, also depends

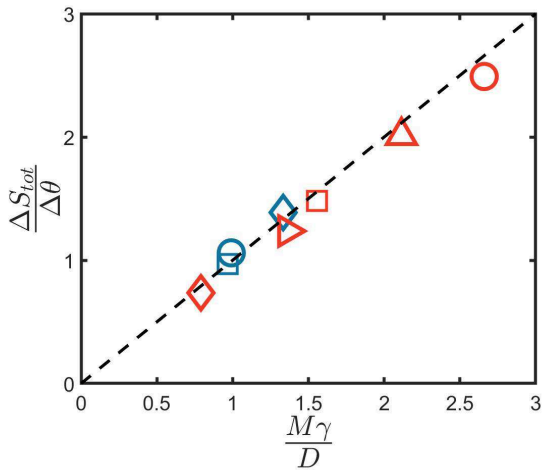

FIG. 5. Fitting parameter $M\gamma/D$ closely relates to $\Delta S/\Delta\theta$, which also explains the slope of symmetry function of Ω_τ (Fig.2). Blue markers stand for experiment and red ones for numerical simulation. Different markers represent different experiment/simulation conditions. Blue square: 15 robots; blue circle: 10 robots; blue star: 15 robots, add silicone oil in rotor bearing, which results in a 20 times higher drag coefficient when rotor rotates. Red square: 10 self- propelled rods; red circle: 15 self-propelled rods; red diamond: 15 self-propelled rods, obtuse angle ratchet; red triangle: 15 self-propelled rods, 75% self-propelling force on each rod; red slant triangle: 15 self-propelled rods, 50% self-propelling force on each rod.

on rotation velocity, as shown in Fig. 4(B)(D): variance for $\Omega_\tau < 0$ is apparently larger than that for $\Omega_\tau > 0$. A probable reason for this dependence is a strong coupling between rotor motion and nearby robots. As shown in our previous publication [27], rotor's counter-clockwise rotation (in positive direction) is able to strongly regularize positions and velocity orientations of outside robots while rotation in negative direction leads to more chaotic outside robot motion, hence larger variance in angular acceleration.

With results on mean and variance for $\mathrm{d}\Omega_\tau$, we can write a discrete time equation for angular velocity

$$\Delta\Omega = (M - \gamma\Omega)\,\Delta t + f\,(\Omega)\,\Delta t\xi, \qquad (6)$$

including a driving term M, a viscous drag γ, and a noise term with variable amplitude $f\,(\Omega)(f(0) = 1)$, $\langle\xi_i \cdot \xi_j\rangle = 2D\delta_{ij}/\Delta t$. M,γ values can be obtained by fitting mean value $\mathrm{d}\Omega_\tau$; D can be estimated by variance of $\mathrm{d}\Omega_\tau$ at $\Omega_\tau = 0$. By Numerically solving Eq. 6, we are able to reproduce major results presented in Fig. 2 and Fig. 3. Distribution of noise term ξ does not have a significant effect on our results. If f is a constant 1, Eq. 6 reduces to a regular Langevin equation which has been well studied [14]; in this case, heat bath temperature can be found as $T = D/\gamma$ and entropy production is related to angular displacement as: $\Delta S{=}M\Delta\theta/T = M\gamma\Delta\theta/D$. Inspired by this result, we plot $\Delta S_{tot}/\Delta\theta$ against $M\gamma/D$ in Fig. 5 and observed a linear relation. This suggests that rotor dynamics in our experiments is governed by a Langevin-like mechanism with a constant drive and a viscous drag. It is possible that D/γ gives an estimation of effective temperature of the heat bath of active robots. Obviously, it requires more experimental and numerical data to determine the significance of such a quantify, which is beyond the scope of our paper.

VI. DISCUSSION AND CONCLUSION

We have studied angular velocity fluctuations of a rotor driven by self-propelled robots. Both experiments and simulations show that relative probabilities of observing rotation in opposite directions are linearly related to angular velocity magnitude. To understand this observation, we constructed a stochastic description of coarse-grained angular velocity time series and showed that the linear dependence found in angular velocity symmetry functions originates from the Fluctuation Relation of stochastic entropy production at the trajectory level. Both probability density functions of entropy production and that of direct measured rotor's angular velocity are non-Gaussian, which is explained by a strong coupling between the orientation of nearby robots and the rotating state of the rotor. Our data also have shown that rotor motion bears strong similarities to Langevin dynamics with a constant driving torque and a linear drag, which explains the linear relation between entropy production and angular displacement in a specific trajectory.

ACKNOWLEDGMENT

We sincerely thank Mingcheng Yang, Zhanchun Tu, David Cai and Xiaqing Shi for helpful discussions.

[1] Evans D J and Searles D J 2002 *Adv. Phys.* **51(7)** 1529-1585

[2] Seifert U 2012 *Rep. Prog. Phys.* **75(12)** 126001

[3] Wang G M, Sevick E M, Mittag E, Searles D J and Evans D J 2002 *Phys. Rev. Lett.* **89(5)** 050601

[4] Garnier N and Ciliberto S 2005 *Phys. Rev. E* **71(6)** 060101

[5] Douarche F, Joubaud S, Garnier N B, Petrosyan A and Ciliberto S 2006 *Phys. Rev. Lett.* **97(14)** 140603

[6] Blickle V, Speck T, Helden L, Seifert U and Bechinger C 2006 *Phys. Rev. Lett.* **96(7)** 070603

[7] Ciliberto S, Garnier N, Hernandez S, Lacpatia C, Pinton J-F and Chavarria G R 2004 *Physica A: Statistical Mechanics and its Applications* **340(1-3)** 204-250

[8] Feitosa K and Menon N 2004 *Phys. Rev. Lett.* **92(16)** 164301

[9] Puglisi A, Visco P, Barrat A, Trizac E and Wijland F v 2005 *Phys. Rev. Lett.* **95(11)** 110202

[10] Shang X D, Tong P and Xia K Q 2005 *Phys. Rev. E* **72(1)** 015301(R)

[11] Majumdar S and Sood A K 2008 *Phys. Rev. Lett.* **101(7)** 078301

[12] Kumar N, Ramaswamy S and Sood A K 2011 *Phys. Rev. Lett.* **106(11)** 118001

[13] Kumar N, Soni H, Ramaswamy S and Sood A K 2015 *Phys. Rev. E* **91(3)** 030102

[14] Joubaud S, Lohse D and Meer D v d 2012 *Phys. Rev. Lett.* **108(21)** 210604

[15] Ramaswamy S 2010 *Annu. Rev. Conden. Ma. P.* **1(1)** 323-345

[16] Marchetti M C, Joanny J F, Ramaswamy S, Liverpool T B, Prost J, Rao M and Simha A 2013 *Rev. Mod. Phys.* **85(3)** 1143-1189

[17] Needleman D and Dogic Z 2017 *Nat. Rev. Mats.* **2(9)** 17048

[18] Bechinger C, Leonardo R Di, Löwen, Reichhardt C, Volpe G and Volpe G 2016 *Rev. Mod. Phys.* **88(4)** 045006

[19] Vicsek T and Zafeiris A 2012 *Physics Reports* **512(3-4)** 71-140

[20] Chen L M 2016 *Acta Physica Sinica* **65(18)** 186401

[21] Romanczuk P, Bär M, Ebeling W, Lindner B and Schimansky-Geier L 2012 *The European Physical Journal Special Topics* **202(1)** 1-162

[22] Wu X L and Libchaber A 2000 *Phys. Rev. Lett.* **84(13)** 3017-3020

[23] Angelani L, Maggi C, Bernardini M L, Rizzo A and Leonardo R Di 2011 *Phys. Rev. Lett.* **107(13))** 138302

[24] Dabelow L, Bo S and Eichhorn R 2019 *Phys. Rev. X* **9(2)** 021009

[25] Pietzonka P, Fodor É, Lohrmann C, Cates M E and Seifert U 2019 *Phys. Rev. X* **9(4)** 041032

[26] Argun A, Moradi A, Pinçe E, Bagci G B, Imparato A and Volpe G 2016 *Phys. Rev. E* **94(6)** 062150

[27] Li H and Zhang H P 2013 *Europhys. Lett.* **102(5)** 50007

[28] Dauchot O and Deméry V 2019 *Phys. Rev. Lett.* **122(6)** 068002

[29] Ciliberto S and Laroche C 1998 *Le Journal de Physique IV* **08(PR6)** Pr6-215 - Pr6-219

[30] Joubaud S, Garnier N B and Ciliberto S 2007 *Journal of Statistical Mechanics: Theory and Experiment* **2007(09)** P09018–P09018

[31] Seifert U 2005 *Phys. Rev. Lett.* **95(4)** 040602

[32] Ford I J and Spinney R E 2012 *Phys. Rev. E* **86(2)** 021127

[33] Spinney R E and Ford I J 2012 *Phys. Rev. Lett.* **108(17)** 170603